Experimental and numerical investigations of rock-concrete interfacial crack propagation under mixed mode I-II fracture

Dong, Wei; Yang, Dong; Zhang, Ben; Wu, Zhimin

Published in:
Journal of Engineering Mechanics

Publication date:
2018

Document Version
Peer reviewed version

Experimental and numerical investigations of rock-concrete interfacial crack propagation under mixed mode I-II fracture

Wei Dong[1,*], Dong Yang[2], Binsheng Zhang[3], Zhimin Wu[4]

[1]Associate Professor, State Key Laboratory of Coastal and Offshore Engineering, Dalian University of Technology & Ocean Engineering Joint Research Centre of DUT-UWA, Dalian 116024, P. R. China. E-mail: dongwei@dlut.edu.cn

*Corresponding author

[2]Postgraduate student, State Key Laboratory of Coastal and Offshore Engineering, Dalian University of Technology, Dalian 116024, P. R. China. E-mail: dongyang@mail.dlut.edu.cn

[3]Professor, Department of Construction and Surveying, School of Engineering and Built Environment, Glasgow Caledonian University, Glasgow G4 0BA, Scotland, United Kingdom. E-mail: Ben.Zhang@gcu.ac.uk

[4]Professor, State Key Laboratory of Coastal and Offshore Engineering, Dalian University of Technology, Dalian 116024, P. R. China. E-mail: wuzhimin@dlut.edu.cn

Abstract

Experimental tests were conducted on the composite rock-concrete specimens with four roughness profiles to investigate the propagation process of interfacial cracks under three-point bending and four-point shear conditions. By measuring the initial fracture loads, various combinations of interfacial stress intensity factors (SIFs) of modes I and II corresponding to the initial fracture conditions were determined. Based on these results, an expression for classifying the initiation of interfacial cracks under the mixed mode I-II fracture was derived by normalization, which could eliminate the effect of interfacial roughness. Furthermore, a criterion for specifying the propagation of the interfacial crack by considering the nonlinear interfacial characteristics was proposed, which indicates that the crack would start to propagate along the interface when the SIFs caused by the external loads and the cohesive stresses satisfied this criterion. The numerical simulations on the interfacial fracture process were also conducted by introducing the crack propagation criterion to predict the load versus crack mouth opening displacement (*P-CMOD*) curves, and a fairly good agreement with the experimental results could be obtained. Finally, by combining the criterion for the maximum circumferential stress with the proposed criterion for crack propagation, the interfacial crack propagation mode was assessed. The results indicated that once the initial fracture toughnesses for the rock, concrete and interface from experimental work were obtained, the propagation process of the interfacial cracks and the corresponding fracture modes including nonlinear characteristics of the materials and interface could be predicted by using the method derived in this study.

Authors' keywords: rock-concrete interface; interface fracture; fracture mode; crack propagation criterion; initial fracture toughness.

Introduction

The operational safety of concrete gravity hydraulic dams is often threatened by the interfacial cracks between the concrete dams and the rock foundations, which are generally caused by the initial defects during construction or complex loading and environmental effects during service. The propagation of these interfacial cracks under hydrostatic pressure will decrease the load-carrying capacity and result in fracture and failure of the structures. In particular, various propagation paths of the interfacial cracks determine failure patterns of concrete dams on rock foundations. Therefore, it is significantly important to predict the fracture process and potential crack trajectory to ensure safety, serviceability and durability of a mass concrete hydraulic dam under service loading conditions.

For a rock-concrete interfacial crack, there are generally three potential propagation paths: (i) propagating fully along the interface until the structure fails; (ii) propagating first along the interface and then kinking into one material; and (iii) kinking into one material after it initiates. It has been verified by experiment that the interfacial crack may follow Path 1 at a low mode mixity ratio K_2/K_1 (Zhong et al. 2014) and is prone to Paths 2 and 3 at a high K_2/K_1 ratio (Slowik et al. 1998). Here, K_1 and K_2 are the stress intensity factors (SIFs) for fracture modes I and II at the tip of an interfacial crack, respectively. However, the crack propagation path is governed not only by the magnitude in the stress field of the crack tip, but also by the material and interface properties. Therefore, for the purpose of the fracture analysis, a criterion for interfacial crack propagation, which can evaluate the balance between the effects of the external loads and the resistance of the materials or interface, should be developed.

So far, a number of criteria have been proposed for the fracture at rock-concrete interface, classified as stress-based (Červenka et al. 1998), energy-based (Qian and Sun 1998, Sujatha and

Kishen 2003) and SIF-based criteria (Kishen and Singh 2001, Zhong et al. 2014, Dong et al. 2016a). For a small fracture process zone (FPZ) at the crack tip, linear elastic fracture mechanics (LEFM) was often employed to establish the criterion and analyze the fracture behavior at the rock-concrete interface (Červenka et al. 1998, Qian and Sun 1998, Sujatha and Kishen 2003, Kishen and Singh 2001, Yang et al. 2008). From a practical point of view, the simplification by disregarding the FPZ is acceptable for a mega structure, e.g. a gravity concrete hydraulic dam on the rock foundation. However, to investigate the fracture mechanism of the bi-material interface, the criterion based nonlinear fracture theory will be more appropriate for assessing the effect of the FPZ on fracture behavior. Particularly, due to the cohesive action on the FPZ, the stress field at the tip of an interfacial crack will change, resulting in transformation of the crack path. In addition, in the case of low mode mixity ratio, the propagation of an interfacial crack was treated as pure mode I fracture. Consequently, the mode I dominated criterion was used to determine crack propagation by assuming the crack path along the interface (Zhong et al. 2014, Dong et al. 2016a). In fact, the propagation of an interfacial crack under mixed mode I-II stress conditions can be predicted by using the formulas including fracture parameters for modes I and II (Slowik et al. 1998). The interface resistance will be over-estimated if only mode I parameter is utilized. Finally, it should be mentioned that some interface fracture criteria were derived only for homogeneous materials, i.e. the maximum circumferential stress (Ryoji and Xu 1992), the net SIF (Moës and Belytschko 2002), and the initial fracture toughness (Dong et al. 2013, Wu et al. 2013). There is a remarkable knowledge gap in the criteria for fracture and failure in homogenous materials and at bi-material interfaces. Hence, a criterion based on the fracture experiment at rock-concrete interface may be more appropriate for fracture analysis of mass concrete structures on rock foundations.

For cementation materials like concrete, the complete fracture process includes three stages: crack initiation, stable propagation and unstable propagation (Xu and Reinhardt 1999a, 1999b). These stages are also applicable for the interface fracture (Dong et al. 2016b). Regarding the cohesive effect on the FPZ under external loading, each step of the propagation of the fictitious crack can be taken as the initiation of a new crack, so that a complete fracture process consists of formations of many new cracks. A criterion used for determining the initiation of a crack can be utilized in the analysis on the crack propagation by introducing the cohesive force acting on the FPZ. This idea has been verified by the numerical simulations of the mode I fracture and mixed I-II fracture of concrete (Dong et al. 2013, Wu et al. 2013). It should be noted that the initiation and propagation of the crack in concrete is still governed by the tensile resistance although the crack tip is under a mixed mode I-II stress state. In these studies, only the initial fracture toughness of mode I was introduced as a material property. However, the scenario is different in the case of the rock-concrete interface under the mixed mode I-II fracture, because the interface is much weaker than the materials on both sides of the crack. Under this condition, the crack is prone to propagating along the interface, rather than being mode I dominated. Therefore, it is a challenge to explore what stress conditions can cause an interfacial crack to propagate, and to predict whether the crack can branch from the interface and kink into a material on one side of the interface.

The objective of this study, therefore, is to develop a criterion for predicting the propagation of the rock-concrete interfacial crack based on the initial fracture toughness and determining potential paths for the propagation of the crack. First, composite rock-concrete specimens with four interfacial roughness profiles are to be tested under three-point bending (TPB) and four-point shear (FPS). By adjusting the loading position in FPS, a wide range of K_2 / K_1 ratios corresponding to the initial cracking load can be obtained. A criterion for specifying the propagation of an interfacial crack based on the initial fracture toughness will then be derived by analyzing the experimental data. Thereafter, the criterion is to be employed in the numerical simulation on the interface fracture and verified by comparing the numerical results with the experimental data. Finally, combining the criterion with the material properties on both sides of the interface, potential crack propagation paths can be determined. It is expected that this investigation is to provide a better understanding of the fracture mechanism for the rock-concrete interface so that the load-carrying capacity and the serviceability and durability of mass concrete structures on rock foundations can be evaluated more accurately.

Experimental Program

Specimen preparation

Two types of specimens were prepared for the experimental study: composite rock-concrete beams and prisms with artificially grooved surfaces for the rock sections. The dimensions of the composite beams for the TPB and FPS tests were 500 mm × 100 mm × 100 mm, while the dimensions of the prism specimens for the direct tension tests were 200 mm × 100 mm × 100 mm. In addition, in order to obtain the fracture parameters of the rock and concrete, individual rock and concrete beams of 500 mm × 100 mm × 100 mm were also prepared for the TPB tests. The geometries of the composite specimens under the TPB and FPS tests are illustrated in Figs. 1(a) and (b). Each composite beam was made up of two portions, i.e. the concrete and rock sections. In the TPB tests, the lengths of the concrete and rock sections were identical, 250 mm each. In the FPS tests, the lengths of the rock sections varied from 225 mm to 250 mm to cover a wide range of mode mixity ratios for the concrete-rock (C-R) series beams. For each composite beam, the length of the pre-crack, a_0, was 30 mm. In order to achieve the pre-crack, two layers of PVC film were put at the location of the pre-crack on the rock, where one PVC film was pasted on the surface of the rock using glue and another one was fixed at the same position using cello tape (see Fig. 2). Then the concrete was cast against the rock section in the mold and the PVC film fixed with cello tape could bond well with the concrete. Before testing, the cello tape was pulled out to eliminate the bonding effect between the two layers of the PVC film.

To obtain the surfaces with various roughness degrees between the rock and concrete, four levels of interfacial roughness were adopted by introducing artificial groove lines on the contact surfaces of the rock sections in this study. The groove lines were parallel to the diagonal lines of the interfacial cross-section with a depth of 3 mm. According to the numbers of groove lines, the side surface was equally divided, and four interfacial roughness profiles were created as 3×3, 4×4, 5×5 and 7×7, respectively, as illustrated in Figs. 3(a) to (d). The degree of roughness, R_a, is quantified by using the sand-filling method (Dong et al. 2016c), and its values are listed in Table 1 where a value of R_a is the average for the composite specimens with the same artificial groove pattern. Fig. 3(e) illustrates the values of the R_a/M_{size} ratio for different roughness profiles where M_{size} is the maximum size of crushed aggregate which was 10 mm for the concrete used in this study.

The rock used for the composite beams was granite, prepared in Dalian, Liaoning Province of China. The composite beams and prisms were fabricated by casting concrete against the rough surfaces of the rock sections. The concrete mix design was cement : water : sand : aggregate = 1:0.60:2.01:3.74 by weight. The composite specimens were demolded one day after casting, and then cured for 28 days in the curing chamber with a 23℃ curing temperature and 90% relative humidity. Three specimens were prepared for each loading condition and roughness profile.

The mechanical properties of the concrete and rock materials and the rock-concrete interfaces are listed in Table1, where E is the elastic modulus, ρ is the density, v is the Poisson's ratio, f_t is the uniaxial tensile strength, f_c is the uniaxial compressive strength, $K_{\mathrm{I}}^{\mathrm{ini}}$ is the initial fracture toughness of mode I, and G_{If} is the fracture energy, respectively. It should be noted that the uniaxial tensile strength of the rock-concrete interface was obtained on the prism specimens tested in direct tension.

TPB and FPS tests

The composite TPB and FPS specimens with four interfacial roughness profiles were tested in a 250 kN closed-loop servo MTS testing machine at a displacement rate of 0.024 mm/min. The experimental setups for the TPB and FPS tests are illustrated in Figs. 4(a) and (b), respectively. The ratio of loads on the two loading points is 1:6 for all C-R series specimens under FPS. The displacement at the loading point, the crack mouth opening displacement (*CMOD*) and the crack mouth sliding displacement (*CMSD*) were measured using clip gauges in the test. In addition, to measure the initial cracking load, two strain gauges were symmetrically put on both sides of the specimen, 5 mm away from the tip of the pre-notch in the ligament. Once the pre-crack began to propagate, the measured strains would drop rapidly due to the sudden release of the stored strain energy at the pre-crack in the specimen. By taking Specimen C-R-240-4×4-1 as an example, Fig. 5 illustrates the relationship between the load and strain at the tip of the pre-crack. It can be seen that the strain reached its maximum at the initial cracking loading P_{ini} = 23.32 kN, and thereafter the strain started to decrease. The decrease in the strain indicates the release of the stored strain energy at the pre-crack tip so that the initial cracking load could be determined.

The experimental results for the TPB and FPS specimens are listed in Tables 2 and 3, respectively. The specimen number "TPB-3×3" in Table 2 denotes the TPB specimen with the 3×3 artificial groove pattern, see Fig. 1(a). G_{If} in Table 2 denotes the fracture energy of mode I fracture for the interfaces with different roughness profiles. The specimen number "C-R-225-3×3" in Table 3 denotes the FPS specimen with the left and right sections as the concrete and rock, respectively. The length for the rock section was 225 mm with the 3×3 artificial groove pattern, see Fig. 1(b). Here, P_{ini} and $P_{\max}$ are the initial and peak loads, and L_R is the length of the rock section. The stress intensity factors K_1 and K_2 for the bi-material interfacial crack were calculated using Eqs. (1) to (7) below (Nagashima et al. 2003). Here, δ_{x} and δ_{y} are the relative crack surface diplacements in the horizontal x and vertical y directions. K_1 and K_2 can be writen as K_1^{ini} and K_2^{ini} when δ_{x} and δ_{y} in Eqs. (1) and (2) are caused by the initial cracking load:

$$K_1 = C \lim_{\mathrm{r}\to 0} \sqrt{\frac{2\pi}{r}} \left[\delta_{\mathrm{y}} \left(\cos Q + 2\varepsilon \sin Q \right) + \delta_{\mathrm{x}} \left(\sin Q - 2\varepsilon \cos Q \right) \right] \tag{1}$$

$$K_2 = C \lim_{r\to 0} \sqrt{\frac{2\pi}{r}} \left[\delta_{y} \left(\cos Q + 2\varepsilon \sin Q \right) - \delta_{x} \left(\sin Q - 2\varepsilon \cos Q \right) \right] \tag{2}$$

where

the constant $$C = \frac{2\cosh(\varepsilon\pi)}{(\kappa_1+1)/\mu_1 + (\kappa_2+1)/\mu_2} \tag{3}$$

the parameter $$Q = \varepsilon \ln r \tag{4}$$

the stiffness parameter $$\varepsilon = \frac{1}{2\pi} \ln \left(\frac{\dfrac{\kappa_1}{\mu_1} + \dfrac{1}{\mu_2}}{\dfrac{\kappa_2}{\mu_2} + \dfrac{1}{\mu_1}} \right) \tag{5}$$

the shear modulii $$\mu_{\mathrm{i}} = \frac{E_{\mathrm{i}}}{2(1+\nu_{\mathrm{i}})} \quad (i = 1, 2) \tag{6}$$

the elastic constants $$\kappa_{\mathrm{i}} = \begin{cases} (3-\nu_{\mathrm{i}})/(1+\nu_{\mathrm{i}}) & \text{(Plane stress)} \\ (3-4\nu_{\mathrm{i}}) & \text{(Plane strain)} \end{cases} \tag{7}$$

E_{i} is the elastic modulus for material i, ν_{i} is the Poisson's ratio for material i, r is the radius of the pre-crack at its tip.

There are two basic failure modes for the composite C-R series beams under FPS. The interface failure mode “I” means that the interfacial crack propagates through the interface until failure occurs. Some C-R series beams which fractured in this failure mode are shown in Fig. 6(a). The other failure mode “IC” was observed on the beams with high mode mixity ratios. Fig. 6(b) shows some examples of this failure mode. In the case of the failure mode “IC”, a sudden brittle failure was observed near the supports at the same time when the interfacial crack propagated through the whole interface. In the case of the failure mode “IC”, the failure at the interior support within the concrete section of the specimen occurred during the unstable fracture process. The initial fracture toughness was calculated based on the initial cracking load, i.e. the failure at the interior support did not occur when the crack initiated. Therefore, the failure mode “IC” did not affect the determination of the initial fracture toughness in this study.

In addition, it is worthwhile to point out that the crack did not propagate exactly along the interfaces. On the artificial grooves of the rock, the crack propagated through the concrete on the grooves (see Fig. 7). For a precise computation, the discrete microstructural model, such as lattice models (Bažant et al. 1990, Gianluca et al. 2003a, 2003b, 2006, 2011a, 2011b), will be a more powerful and realistic alternative for simulating the softening damage and fracture of concrete. In these models, the concrete was sub-divided into mortar, aggregate and the interface between them, and these sub-components can be described as mesoscopic elements. Various meso-structural characteristics, such as aggregate size and distribution, and stress and strain fields in the meso-structure, can be directly simulated. In this study, the concrete was modeled as the homogeneous materials and this study was conducted from macroscopic perspectives rather than mesoscopic ones. The interfacial fracture energy and fracture toughness reflect the fracture charateristics at the interface on average. The effect of the interfacial roughness profile is considered through measuring the fracture energy and fracture toughness of the specimens with the same degree of roughness. These fracture parameters to be used in the following numerical simulations also corresponded to those from the specimens with the same degree of roughness.

Criterion for Crack Propagation and Experimental Verification

Criterion for crack propagation

From the experimental results, it can be found that the interfacial cracks can initiate under different combinations of K_1^{ini} and K_2^{ini}. When the interfacial fracture was pure mode I, the crack initiation would be determined by the intial mode I fracture toughness, K_{1C}^{ini}, i.e. $K_1^{\text{ini}} = K_{1C}^{\text{ini}}$ and $K_2^{\text{ini}} = 0$. When the fracture mode of interface was pure mode II, the crack initiation would be determined by the intial mode II fracture toughness, K_2^{ini}, i.e. $K_1^{\text{ini}} = 0$ and $K_2^{\text{ini}} = K_{2C}^{\text{ini}}$. In addition, in the cases of mixed mode I-II intefacial fracture, $K_1^{\text{ini}} < K_{1C}^{\text{ini}}$ and $K_2^{\text{ini}} < K_{2C}^{\text{ini}}$. The mode mixity ratio, $K_2^{\text{ini}} / K_1^{\text{ini}}$, represents the relationship between the tensile and shear stresses at the tip of the interfacial crack. If all the combinations of K_1^{ini} and K_2^{ini} are grouped to form an envelope, it will represent the crack initiation conditions under various combinations of tensile and shear stresses. Thus, the equation for the curve with the parameters K_1^{ini} and K_2^{ini} would become the criterion for the initiation of a crack. Through careful experimental design, a wide range of $K_2^{\text{ini}} / K_1^{\text{ini}}$ ratios could be derived from the TPB and FPS tests, varying from 0.055 to 16.595, as illustrated Tables 2 and 3. Furthermore, the effect of the interface roughness on the crtierion for the crack initiation was investigated by testing the composite specimens with four roughness profiles. Fig. 8 illustrates the relationships between K_1^{ini} and K_2^{ini} from the testing data with various interface roughness degrees and the fitted curves. It can be seen that the K_1^{ini} versus K_2^{ini} curve would move outward when R_{a} increased from 0.780 to 1.548, indicating that the interfacial cracking resistance would indeed increase with the increasing interfacial roughness.

To derive the equation for the initial fracture by eliminating the effect of roughness degree, the normalizing method was utilized by dividing K_1^{ini} and K_2^{ini} by the corresponding $K_{1\mathrm{C}}^{\mathrm{ini}}$ for each test series with the same R_{a}. The points for the normalized terms $K_1^{\mathrm{ini}} / K_{1\mathrm{C}}^{\mathrm{ini}}$ and $K_2^{\mathrm{ini}} / K_{1\mathrm{C}}^{\mathrm{ini}}$ with various values of R_{a} are shown in Fig. 9. It can be seen that the effect of the interface roughness could be eliminated approximately through the normalizing process. Therefore, the regressive equation for the initial fracture could be derived by fitting all the scattered testing points as Eq. (8), where the shape of the equation for the initiation of the interfacial crack would be a quarter-ellipse, with the ratio of the long axial length to the short axial length as 1.6, i.e.

$$\left(\frac{K_1}{K_{1\mathrm{C}}^{\mathrm{ini}}}\right)^2 + \left(\frac{K_2}{1.6\,K_{1\mathrm{C}}^{\mathrm{ini}}}\right)^2 = 1 \tag{8}$$

If a complete fracture process could be regarded as crack propagation for many steps, each step for the propagation of the existing crack would be regarded as the initiation of a new crack. Then, the crack initiation equation could be used to predict the crack propagation at interface. However, considering the nonlinear characteristics of the rock-concrete interface, there are cohesive stresses acting on the FPZ of the interfacial crack according to the fictious cracking model (Hillerborg et al. 1976). Therefore, when the equation for the crack initiation was used to predict the propagation process of the crack, the SIFs, K_1 and K_2, would be governed by the external load and the cohesive force of the PFZ, i.e. $K_1 = K_1^{\mathrm{P}} - K_1^{\sigma,\tau}$ and $K_2 = K_2^{\mathrm{P}} - K_2^{\sigma,\tau}$. Here, K_1^{P} and K_2^{P} are the SIFs of modes I and II caused by the external load, while $K_1^{\sigma,\tau}$ and $K_2^{\sigma,\tau}$ are the SIFs of modes I and II caused by the cohesive tensile and shear stresses on the FPZ, σ and τ. Thus, Eq. (8) can be rewritten as Eq. (9) when it is used to determine the propagation of the crack along the interface, with $K_{1,2}^{*}$ representing the function of the criterion for the proapgation of the interficial crack:

$$K_{1,2}^{*}=\sqrt{\left(\frac{K_1^{\mathrm{P}}-K_1^{\sigma,\tau}}{1}\right)^2+\left(\frac{K_2^{\mathrm{P}}-K_2^{\sigma,\tau}}{1.6}\right)^2}=K_{1\mathrm{C}}^{\mathrm{ini}} \tag{9}$$

In the case of mode I interface fracture, K_2 and the cohesive shear stress are equal to 0 so that Eq. (9) will be degenerated to:

$$K_1^{\mathrm{P}}-K_1^{\sigma}=K_{1\mathrm{C}}^{\mathrm{ini}} \tag{10}$$

Eq. (10) is the criterion of the crack propagation for the mode I interface fracture, which is a particular case of the mixed mode I-II fracture and has been verified in the previous research (Dong et al. 2016a).

Application and experimental verification

In order to verify the derived criterion for the propagation of the interfacial crack, numerical simulations based on the fictitious cracking model were conducted to predict the fracture process of the composite rock-concrete beams under TPB and FPS. The finite element analyses were carried out using commercial software ANSYS. The cohesive traction-displacement relationships for tension and shear softening are illustrated in Figs. 10(a) and (b), respectively. In Fig. 10(a), the crack opening displacement (COD) at the breaking point on the bi-linear σ-w curve, w_{n0}, and the corresponding cohesive stress, σ_{n0}, were set as $0.8G_{\mathrm{If}}/f_{\mathrm{t}}$ and $0.2f_{\mathrm{t}}$, respectively. The stress-free COD, w_{nc}, was set as $6G_{\mathrm{If}}/f_{\mathrm{t}}$ (Dong et al. 2016c). In Fig. 10(b), the crack slip displacement (CSD) at the breaking point on the bi-linear τ-w curve, w_{s0}, and the corresponding interface shear strength, τ_{s0}, were set as 0.002 mm and $7f_{\mathrm{t}}/4$, respectively. The stress-free CSD, w_{sc}, was set as $2G_{\mathrm{IIf}}/\tau_{\mathrm{s0}}$. Here, G_{IIf} is the mode II interface fracture energy, which was set to be equal to $2G_{\mathrm{If}}$ (Zhong et al. 2014).

If a pre-crack is assumed to initiate and propagate fully along the interface, the criterion for the crack propagation can be used to predict the complete fracture process under the mixed mode I-II fracture. Fig. 11 illustrates the flow chart for the program, and the numerical simulation procedure is summarized as follows:

1. Establish the finite element model with the crack length $a_{i,j} = a_0 + (j - 1)\cdot\Delta a$ (i = 1, 2…; j = 2, 3…). Here a_0 is the initial crack length, Δa is a specified increment of the crack length, i represents the load increment during the iteration process with a fixed crack length, and j represents the increment of the crack length during the iterations.
2. Apply the load $P_{i,j}$ and calculate the cohesive stresses $\sigma_{i,j}$ and $\tau_{i,j}$ according to the cohesive tensile/shear traction – displacement relationships as shown in Fig. 10.
3. Calculate K_1^{P}, $K_1^{\sigma,\tau}$, K_2^{P} and $K_2^{\sigma,\tau}$ by adjusting load $P_{i,j} = P_{i-1,j} \pm \Delta P$ until Eq. (9) is satisfied.
4. Repeat Steps 1 and 3 for the next step of crack propagation.
5. Terminate the iterative process when $a_{i,j}$ is equal to the specimen height or $P_{i,j} \leq 0$.

By repeating the steps, the complete interface fracture process can be obtained numerically. The parameters used in the simulations included K_1^{ini} and G_{If}, which have been listed in Tables 1 and 2. By taking Specimens TPB-5×5, C-R-240-3×3, C-R-240-4×4, C-R-235-5×5 and C-R-250-7×7 as examples, Fig. 12 illustrates the comparisons of the numerically predicted *P-CMOD* curves with the experimental data, and fairly good agreements can be observed.

Discussion on Crack Propagation Paths

As motioned above, three potential propagation paths existed for the pre-crack at the rock-concrete interface, which would be governed by the stress conditions in front of the crack tip and the mechanical properties of the concrete, rock and their interface. Generally, the mechanical and fracture properties of the interface were smaller than those for the concrete and rock. Therefore, the crack would propagate along the interface in the mode I dominated fracture. With the increase of K_2/K_1, the crack could branch at the interface and kink into the rock or concrete, even the crack directly initiated in the rock or concrete. To predict the potential crack propagation path, in addition to the criterion for the propagation of the interfacial crack, it is also essential to develop the criterion for the crack to penetrate into the rock or concrete.

In this study, the function for the maximum circumferential stress criterion (Ryoji and Xu 1992, Kishen and Singh 2001) was employed to determine the kinking of the interfacial crack as follows:

$$K^{*}_{\mathrm{I,II}} = \frac{\sqrt{(K_1^{\mathrm{P}} - K_1^{\sigma,\tau})^2 + (K_2^{\mathrm{P}} - K_2^{\sigma,\tau})^2}}{2\cosh(\varepsilon\pi)} W_{\mathrm{j}} \left[2\cos\left(\frac{\theta_0}{2} + \gamma\right) - (\cos\theta_0 + 2\varepsilon\sin\theta_0)\cos\left(\frac{\theta_0}{2} - \gamma\right) \right] + \frac{1}{W_{\mathrm{j}}}\cos\left(\frac{3}{2}\theta_0 + \gamma\right) = K_{\mathrm{Ij}}^{\mathrm{ini}} \tag{11}$$

where $K_{\mathrm{Ij}}^{\mathrm{ini}}$ is the initial mode I fracture toughness of material j, j denotes rock or concrete, and θ_0 is the kinking angle which can be obtained by solving Eq. (12) numerically

$$\begin{aligned} &\varepsilon W_{\mathrm{j}} \left[2\cos\left(\frac{\theta}{2} + \gamma\right) - (\cos\theta + 2\varepsilon\sin\theta)\cos\left(\frac{\theta}{2} - \gamma\right) \right] \\ &+ W_{\mathrm{j}} \left[-\sin\left(\frac{\theta}{2} + \gamma\right) + (\sin\theta - 2\varepsilon\cos\theta)\cos\left(\frac{\theta}{2} - \gamma\right) \right] \\ &+ W_{\mathrm{j}} \left[\frac{1}{2}(\cos\theta + 2\varepsilon\sin\theta)\sin\left(\frac{\theta}{2} - \gamma\right) \right] - \frac{1}{W_{\mathrm{j}}} \left[\varepsilon\cos\left(\frac{3}{2}\theta + \gamma\right) + \frac{3}{2}\sin\left(\frac{3}{2}\theta + \gamma\right) \right] = 0 \end{aligned} \tag{12}$$

with
$$\gamma = \begin{cases} \arctan((K_2^{\mathrm{P}} - K_2^{\sigma,\tau}) / (K_2^{\mathrm{P}} - K_2^{\sigma,\tau})) & K_1 > 0 \\ \pi + \arctan((K_2^{\mathrm{P}} - K_2^{\sigma,\tau}) / (K_2^{\mathrm{P}} - K_2^{\sigma,\tau})) & K_1 < 0 \end{cases} \tag{13}$$

$$W_{\mathrm{j}} = \begin{cases} e^{-\varepsilon(\pi - \theta_0)} & j = 1 \\ e^{\varepsilon(\pi + \theta_0)} & j = 2 \end{cases} \tag{14}$$

It should be mentioned that the expression for the maximum circumferential stress criterion used in this study is different from those in literature (Ryoji and Xu 1992, Kishen and Singh 2001). Instead of the unstable fracture toughness K_{ICj}, the initial fracture toughness $K_{\mathrm{Ij}}^{\mathrm{ini}}$, which is on the right side of Eq. (11) was used to determine the crack initiation. The purpose of the substitution is considering that the crack propagation into the material *j* still represents the initiation of a new crack rather than the unstable propagation of the existing crack. In addition, Eq. (11) can only be obtained for small $|\varepsilon|$ (Ryoji and Xu 1992). Here, ε is a material constant shown in Eq. (5). Fortunately, the value of $|\varepsilon|$ for dissimilar composite materials is less than 0.1. For instance, the value of $|\varepsilon|$ for the composite rock-concrete specimens in this study was calculated as 0.0074, so that the criterion shown in Eq. (11) should be valid.

By combining the criterion equation for the propagation of the interfacial crack, i.e. Eq. (9), with the criterion equation for the maximum circumferential stress of material *j*, i.e. Eq. (11), the potential propagation of an interfacial crack could be judged in this study as follows:

(i) If $K_{\mathrm{I,II}}^{*} < K_{\mathrm{Ij}}^{\mathrm{ini}}$ and $K_{1,2}^{*} < K_{1\mathrm{C}}^{\mathrm{ini}}$, the crack does not propagate;

(ii) If $K_{\mathrm{I,II}}^{*} < K_{\mathrm{Ij}}^{\mathrm{ini}}$ and $K_{1,2}^{*} > K_{1\mathrm{C}}^{\mathrm{ini}}$, the crack propagates along the interface;

(iii) If $K_{\mathrm{I,II}}^{*} > K_{\mathrm{Ij}}^{\mathrm{ini}}$ and $K_{1,2}^{*} < K_{1\mathrm{C}}^{\mathrm{ini}}$, the crack propagates into the material *j* with a kinking angle θ_0.

The above mentioned method can be also used to predict the crack initiation. In this case, only the SIFs caused by the external load, i.e. K_1^{P} and K_2^{P}, exist in the expressions for $K_{\mathrm{I,II}}^{*}$ and $K_{1,2}^{*}$, due to no development of micro-cracks. Therefore, the crack will directly penetrate into the material *j* if $K_{\mathrm{I,II}}^{*} > K_{\mathrm{Ij}}^{\mathrm{ini}}$ and $K_{1,2}^{*} < K_{1\mathrm{C}}^{\mathrm{ini}}$. Under this condition, the fracture analysis transforms into the crack propagation in a homogeneous material under the mixed mode I-II loading, which has been investigated by Wu et al. (2013).

In addition, the potential crack propagation path could be predicted by applying the criteria for the propagation of the interfacial crack and the maximum circumferential stress. By taking the composite C-R series beams in this study as examples, Fig. 13(a) shows the $K_1 - K_2$ relationships of the criteria with $K_{\mathrm{I,II}}^{*} = K_{\mathrm{Ij}}^{\mathrm{ini}}$ for the rock and $K_{1,2}^{*} = K_{1\mathrm{C}}^{\mathrm{ini}}$ for the interface. For the composite C-R series beams under the loading condition as shown in Fig. 1(b), it is impossible for the crack to kink into the concrete so that only the criterion for the interfacial crack propagation and the criterion for the maximum circumferential stress of the rock were assessed. For the criterion for the interfacial crack initiation, i.e. $K_{1,2}^{*} = K_{1\mathrm{C}}^{\mathrm{ini}}$, there were four curves with respect to the interfaces of four roughness degrees, as illustrated in Fig. 13(a). For the criterion for the maximum circumferential stress of the rock, i.e. $K_{\mathrm{I,II}}^{*} = K_{\mathrm{Ij}}^{\mathrm{ini}}$ with j representing the rock, there is one curve illustrated in Fig. 13(a). $K_{\mathrm{Ij}}^{\mathrm{ini}}$ for the rock in this study was determined as 1.205 MPa·m$^{1/2}$ by conducting the standard TPB tests on the rock specimens. It can be seen from this figure that the curve for the rock with $K_{\mathrm{I,II}}^{*} = K_{\mathrm{Ij}}^{\mathrm{ini}}$ is always outside the curves for $K_{1,2}^{*} = K_{1\mathrm{C}}^{\mathrm{ini}}$. This indicates that under any loading conditions, the crack would not propagate into the rock from the interfaces of the composite C-R specimens with four roughness degrees in this study. This has also been validated by the experimental failure patterns of the composite C-R series beams as shown in Fig. 6. The qualitative assessment is significantly useful for practical constructions, e.g. gravity concrete hydraulic dams, to determine whether propagations of interfacial cracks into rock foundations can be excluded or not.

It should be mentioned that, even though the crack propagated fully along the interface for all composite C-R series beams, there would still exist two different variation tendencies for K_2/K_1 during the complete fracture process. One is that the ratio K_2/K_1 would always increase as the interfacial crack propagated, and another is that the ratio would always decrease correspondingly.

Based on the numerical simulation results, it is found that there was a critical value for the mode mixity ratio K_2/K_1 when the material and interface properties were given. This critical mode mixity ratio was equal to 0.788 for the materials adopted in this study. The points for four toughness degrees corresponding to the critical mode mixity ratio are illustrated in Fig. 13(a) as A, B, C and D, respectively. When the ratio $K_2^{\mathrm{ini}}/K_1^{\mathrm{ini}}$ was less than the critical value, the ratio K_2/K_1 would always decrease as the crack propagated so that the fracture became mode I dominated. In contrast, when the ratio $K_2^{\mathrm{ini}}/K_1^{\mathrm{ini}}$ was greater than the critical value, the ratio K_2/K_1 would always increase as the crack propagated and the fracture became mode II dominated. Fig. 13(a) also shows the variations of K_2/K_1 during the crack propagation for the C-R-235 series specimens with $K_2^{\mathrm{ini}}/K_1^{\mathrm{ini}} = 0.718 < 0.788$ (see the solid symbols in Fig. 13(a)), and for the C-R-245 series specimens with $K_2^{\mathrm{ini}}/K_1^{\mathrm{ini}} = 2.275 > 0.788$ (see the hollow symbols). This clearly illustrates the variation tendencies of K_2/K_1 for the specimens with different values of $K_2^{\mathrm{ini}}/K_1^{\mathrm{ini}}$ during the complete fracture process.

Although the interfacial crack does not propagate into the rock based on the criterion comparisons in Fig. 13(a), the propagation path of the interfacial crack can still not be defined if the positions of the rock and concrete are exchanged. In this case, the relationship between the criterion for the maximum circumferential stress of the concrete and the criterion for the propagation of the interfacial crack should be evaluated. The curves for the criteria with $K_{\mathrm{I,II}}^{*} = K_{\mathrm{Ij}}^{\mathrm{ini}}$ and $K_{1,2}^{*} = K_{\mathrm{1C}}^{\mathrm{ini}}$ are shown in Fig. 13(b), where j denotes the concrete material. For the criterion with $K_{1,2}^{*} = K_{\mathrm{1C}}^{\mathrm{ini}}$, the curves with respect to two toughness degrees (R_{a} = 0.963 and $K_{\mathrm{1C}}^{\mathrm{ini}} = 0.399$; R_{a} = 1.183, $K_{\mathrm{1C}}^{\mathrm{ini}} = 0.450$) are illustrated as examples. For the criterion with $K_{\mathrm{I,II}}^{*} = K_{\mathrm{Ij}}^{\mathrm{ini}}$, $K_{\mathrm{Ij}}^{\mathrm{ini}}$ for the concrete was determined as 0.55 MPam$^{1/2}$ from the standard TPB tests on the concrete specimens. Compared with the curves in Fig. 13(a), the criterion curve for the interface intersected with the curve for the concrete in Fig. 13(b). The intersection points corresponded to different K_2/K_1 ratios, i.e. P_C = 0.764 (R_a= 0.963 and $K_{1C}^{ini} = 0.399$) and Q_C = 0.509 (R_a= 1.183 and $K_{1C}^{ini} = 0.450$). This indicates that the interfacial crack would directly initiate and propagate into concrete when $K_2^{ini} / K_1^{ini} > 0.764$ for R_a = 0.963 and $K_2^{ini} / K_1^{ini} > 0.509$ for R_a= 1.183. In contrast, the interfacial crack would initiate and propagate along the interface when $K_2^{ini} / K_1^{ini} < 0.764$ for R_a= 0.963 and $K_2^{ini} / K_1^{ini} < 0.509$ for R_a = 1.183. In addition, it is worthwhile to discuss whether an interfacial crack could kink into the concrete after propagating along the interface. Based on the previous investigations, the variations in K_2/K_1 in the case of interfacial propagation were determined by the critical mode mixty ratio, which are marked as Points B and C in Fig. 13(b). The intersection points Q_C and P_C are on the left of the critical points C and B, respectively. It indicates that, in the cases of $K_2^{ini} / K_1^{ini} < 0.764$ (Point Q_C) for R_a = 0.963 and $K_2^{ini} / K_1^{ini} < 0.509$ (Point P_C) for R_a = 1.183, the K_2/K_1 ratio would increase as the interfacial crack propagates so that it would not propagate into the concrete under this condition.

In order to verify the crack propagation in this case, the composite rock-concrete (R-C) series beams were prepared with two interfacial roughness degrees, i.e. R_a = 0.963 and 1.183. The geometric properties of the R-C series specimens are shown in Fig. 14. It should be noted that, compared with the C-R series specimens shown in Fig. 1(b), the positions of the rock and concrete in the R-C series specimens were exchanged so that the crack could propagate along the interface or penetrate into the concrete under this loading condition. The K_2^{ini}/K_1^{ini} ratios were determined as 0.788 and 0.696 for R_a = 0.963, and 0.531 and 0.437 for R_a = 1.183 (see Table 4). The corresponding points are denoted as P_2, P_1, Q_2 and Q_1 in Fig. 13(b), respectively. The experimental design ensured that the K_2^{ini}/K_1^{ini} ratios for the test points would be on both sides of the criterion intersection points for the same R_a. The experimental results are listed in Table 4. For the R-C series specimens, the initiation and propagation of the crack in the concrete were observed on Specimens R-C-264-4×4 (Point P_2 with $K_2^{\text{ini}} / K_1^{\text{ini}} = 0.788$) and R-C-271-5×5 (Point Q_2 with $K_2^{\text{ini}} / K_1^{\text{ini}} = 0.531$), which is denoted as the failure mode K in Table 4. Correspondingly, the crack propagations fully along the interface were observed on Specimens R-C-266-4×4 (Point P_1 with $K_2^{\text{ini}} / K_1^{\text{ini}} = 0.696$) and R-C-275-5×5 (Point Q_1 of $K_2^{\text{ini}} / K_1^{\text{ini}} = 0.437$), which is denoted as the failure mode I. Fig. 15 shows the failure mode with the initiation and propagation of the crack into the concrete. By taking Specimen R-C-264-4×4 as an example, Figs. 16(a) and (b) illustrate the comparison of the *P-CMOD* curves and the crack propagation trajectories between the experimental and numerical results, respectively, and reasonably good agreements can be observed.

The investigations in this study indicate that the crack propagation mode under different stress conditions could be predicted by combining Eqs. (9) and (11). The application of the proposed predicting method is convenient because only three initial fracture toughnesses for the rock and concrete materials and their interface would be required in these two equations. Particularly, the three initial fracture toughnesses are relatively easily obtained from the experiment (Dong et al. 2013, Dong et al. 2016c). Once the curves for Eqs. (9) and (11) are obtained, therefore, the failure mode for a mass concrete structure on the rock foundation can be approximately assessed according the loading conditions. However, it should be noted that the further work is still needed to investigate whether Eq. (9) is appropriate for concretes and rocks with various strengths and compositions.

Conclusions

To study the propagation process of the rock-concrete interfacial crack, an expression for the initiation of the interfacial crack has been derived from the experimental investigations. By taking into account the nonlinear characteristics of the interface between two different materials, a criterion for the crack propagation has been proposed to envisage the propagation of a crack along the interface. Based on the criterion for the maximum circumferential stress and the proposed criterion in this study, the interfacial fracture modes, including propagating of a crack along the interface and kinking into the rock or concrete, can be predicted by analyzing the verification curves for these two criteria simultaneously. According to the comprehensive experimental and numerical investigations, the following conclusions can be drawn:

1. For the rock-concrete interfaces with four different roughness profiles investigated in this study, a universal expression for predicting the initiation of a crack along the interface has been obtained by normalizing their initial fracture toughnesses. Also, a criterion for the propagation of the crack has been proposed based on the expression for the crack initiation by introducing the fictitious crack model. This criterion has been verified by comparing the *P-CMOD* curves obtained numerically and experimentally, and fairly good agreements have been observed. However, further work should be conducted to verify the validity of the universal expression for the initiation of a crack at the interfaces between concrete and rock of different properties and compositions.
2. The proposed criterion for the propagation of the interfacial crack can be utilized to predict the complete interfacial fracture process for the mixed mode I-II fracture. By applying the fictitious cracking model, the nonlinear characteristics of the interface have been considered in the criterion. This has been verified by comparing the *P-CMOD* curves obtained from the experimental investigations and numerical simulations. For propagation of the crack along the

interface, there exists a critical mode mixty ratio, which has been determined as 0.788 for the materials used in this study. When the $K_2^{\text{ini}} / K_1^{\text{ini}}$ ratio was greater than the critical mode mixty ratio, K_2/K_1 would increase as the interfacial crack propagated. In contrast, when the $K_2^{\text{ini}} / K_1^{\text{ini}}$ ratio was less than the critical mixty ratio, the K_2/K_1 ratio would decrease as the interfacial crack propagated.

3. Crack propagation paths, i.e. developing along the interface or kinking into the rock or concrete, could be predicted by analyzing the curves for the criterion for the interfacial crack propagation and the criterion for the crack to kink into the rock or concrete. If the curve for the interfacial criterion was inside the curve for the kinking criterion for the rock or concrete, the crack would always propagate along the interface. In contrast, if there was an intersection point between two criteria, the interfacial crack would either propagate along the interface or penetrate into rock or concrete, depending on the relationship between the $K_2^{\text{ini}} / K_1^{\text{ini}}$ ratio and the K_2/K_1 ratio corresponding to the intersection point.
4. The criteria for propagating and kinking of the interfacial crack into the rock or concrete could be determined by obtaining the initial fracture toughnesses of the rock, concrete and their interface. Actually, these values could be conveniently derived by measuring the initial fracture load from the TPB tests.

Acknowledgements

The financial support of the National Natural Science Foundation of China under the grants of NSFC 51478083, NSFC 51421064 and NSFC 51109026, the Fundamental Research Funds for the Central Universities of China under the grants of DUT17LK06, and the Natural Science Foundation of Liaoning Province of China under the grant of 20170540183 is gratefully acknowledged.

References

Bažant, Z. P., M. R. Tabbara, M. T. Kazemi and G. Pijaudier-Cabot (1990). "Random particle model for fracture of aggregate or fiber composites." *J. Eng. Mech.*, **116**(8), 1686-1705.

Červenka, J., J. C. Kishen and V. E. Saouma (1998). "Mixed mode fracture of cementitious bimaterial interfaces: Part II Numerical simulation." *Eng. Fract. Mech.*, **60**(1), 95-107.

Cusatis, G., Z. P. Bažant and L. Cedolin (2003a). "Confinement-shear lattice model for concrete damage in tension and compression: II. Computation and validation." *J. Eng. Mech.*, **129**(12), 1449-1458.

Cusatis, G., Z. P. Bažant and L. Cedolin (2003b). "Confinement-shear lattice model for concrete damage in tension and compression: I. Theory." *J. Eng. Mech.*, **129**(12), 1439-1448.

Cusatis, G., Z. P. Bažant and L. Cedolin (2006). "Confinement-shear lattice CSL model for fracture propagation in concrete." *Computer Methods in Applied Mechanics and Engineering*, **195**(52), 7154-7171.

Cusatis, G., A. Mencarelli, D. Pelessone and J. Baylot (2011a). "Lattice discrete particle model (LDPM) for failure behavior of concrete. II: Calibration and validation." *Cement and Concrete composites*, **33**(9), 891-905.

Cusatis, G., D. Pelessone and A. Mencarelli (2011b). "Lattice discrete particle model (LDPM) for failure behavior of concrete. I: Theory." *Cement and Concrete Composites*, **33**(9), 881-890.

Dong, W., Z. Wu and X. Zhou (2013). "Calculating crack extension resistance of concrete based on a new crack propagation criterion." *Constr. Build. Mater.*, **38**, 879-889.

Dong, W., D. Yang, X. Zhou, G. Kastiukas and B. Zhang (2016a). "Experimental and numerical investigations on fracture process zone of rock–concrete interface." *Fatigue Fract. Eng. M.* (in press).

Dong, W., Z. Wu, X. Zhou, N. Wang and G. Kastiukas (2016b). "An experimental study on crack propagation at rock-concrete interface using digital image correlation technique." *Eng. Fract. Mech.* (in press).

Dong, W., Z. Wu and X. Zhou (2016c). "Fracture mechanisms of rock-concrete interface: experimental and numerical." *J. Eng. Mech.*, **142**(7), 04016040.

Hillerborg, A., M. Modéer and P.-E. Petersson (1976). "Analysis of crack formation and crack growth in concrete by means of fracture mechanics and finite elements." *Cem. Conc. Res.*, **6**(6), 773-781.

Kishen, J. C. and K. D. Singh (2001). "Stress intensity factors based fracture criteria for kinking and branching of interface crack: application to dams." *Eng. Fract. Mech.*, **68**(2), 201-219.

Moës, N. and T. Belytschko (2002). "Extended finite element method for cohesive crack growth." *Eng. Fract. Mech.*, **69**(7), 813-833.

Nagashima, T., Y. Omoto and S. Tani (2003). "Stress intensity factor analysis of interface cracks using X-FEM." *Int. J. for Num. Methods in Eng.*, **56**(8), 1151-1173.

Qian, W. and C. Sun (1998). "Methods for calculating stress intensity factors for interfacial cracks between two orthotropic solids." *Int. J. Solids Struct.*, **35**(25), 3317-3330.

Ryoji, Y. and J.-Q. Xu (1992). "Stress based criterion for an interface crack kinking out of the interface in dissimilar materials." *Eng. Fract. Mech.*, **41**(5), 635-644.

Slowik, V., J. C. Kishen and V. E. Saouma (1998). "Mixed mode fracture of cementitious bimaterial interfaces: Part I Experimental results." *Eng. Fract. Mech.*, **60**(1), 83-94.

Sujatha, V. and J. C. Kishen (2003). "Energy release rate due to friction at bimaterial interface in dams." *J. Eng. Mech.*, **129**(7), 793-800.

Wu, Z., H. Rong, J. Zheng and W. Dong (2013). "Numerical method for mixed-mode I–II crack propagation in concrete." *J. Eng. Mech.*, **139**(11), 1530-1538.

Xu, S. and H. W. Reinhardt (1999a). "Determination of double-K criterion for crack propagation in quasi-brittle fracture: Part I Experimental investigation of crack propagation." *Int. J. Fract.*, **98**(2), 111-149.

Xu, S. and H. W. Reinhardt (1999b). "Determination of double-K criterion for crack propagation in quasi-brittle fracture: Part II Analytical evaluating and practical measuring methods for three-point bending notched beams." *Int. J. Fract.*, **98**(2), 151-177.

Yang, S., L. Song, Z. Li and S. Huang (2008). "Experimental investigation on fracture toughness of interface crack for rock/concrete." *Int. J. Mod. Phys. B*, **22**(31/32), 6141-6148.

Zhong, H., E. T. Ooi, C. Song, T. Ding, G. Lin and H. Li (2014). "Experimental and numerical study of the dependency of interface fracture in concrete–rock specimens on mode mixity." *Eng. Fract. Mech.*, **124**, 287-309.

Tables

Table 1 Mechanical properties of concrete and rock materials and their interfaces[1].

Series	E (GPa)	ρ (g/cm^3)	ν	f_t (MPa)	f_c (MPa)	R_a (mm)	K_I^{ini} (MPa·m$^{1/2}$)	G_{If} (N/m)
Concrete	32.86	2.45	0.256	2.200	37.20		0.550	101.91
Rock	41.17	2.75	0.173	-	142.00		1.205	135.38
Interface (3×3)	-	-	-	1.170	-	0.780	-	-
Interface (4×4)	-	-	-	1.391	-	0.963	-	-
Interface (5×5)	-	-	-	1.659	-	1.183	-	-
Interface (7×7)	-	-	-	2.101	-	1.548	-	-

[1] E – Elastic modulus; ρ – Density; ν – Poisson's ratio; f_t – Uniaxial tensile strength; f_c – Uniaxial compressive strength; R_a – Degree of roughness; K_I^{ini} – Initial fracture toughness of mode I; G_{If} – Fracture energy.

Table 2 Experimental results of the TPB tests[2].

Specimen	P_{ini} (kN)	P_{max} (kN)	K_1^{ini} (MPa·m$^{1/2}$)	K_2^{ini} (MPa·m$^{1/2}$)	$\lvert K_2^{ini} / K_1^{ini} \rvert$	R_a (mm)	G_{If} (N/m)
TPB-3×3	1.720	1.825	0.351	-0.019	0.055	0.780	9.25
TPB-4×4	1.965	2.234	0.399	-0.022	0.055	0.963	18.98
TPB-5×5	2.210	2.623	0.450	-0.025	0.055	1.183	22.72
TPB-7×7	2.385	2.816	0.483	-0.026	0.055	1.548	30.14

[2] P_{ini} – Initial cracking load; P_{max} – Peak load; K_1^{ini} – Initial fracture toughness of mode 1; K_2^{ini} – Initial fracture toughness of mode 2; R_a – Degree of roughness; G_{If} – Fracture energy.

Table 3 Experimental results of the C-R series beams under FPS[3].

Specimen	L_R (mm)	P_{ini} (kN)	P_{max} (kN)	K_1^{ini} (MPa·m$^{1/2}$)	K_2^{ini} (MPa·m$^{1/2}$)	$\lvert K_2^{ini} / K_1^{ini} \rvert$	R_a (mm)	Failure mode
C-R-225-3×3	225	12.860	14.947	0.399	0.143	0.359		I
C-R-235-3×3	235	14.136	18.813	0.298	0.215	0.723		I
C-R-240-3×3	240	22.000	22.545	0.334	0.381	1.138	0.780	I
C-R-245-3×3	245	27.065	27.865	0.232	0.528	2.275		I
C-R-250-3×3	250	27.500	37.087	0.036	0.606	16.595		I
C-R-225-4×4	225	13.405	15.355	0.416	0.149	0.358		I
C-R-235-4×4	235	17.080	20.687	0.361	0.260	0.719		I
C-R-240-4×4	240	23.990	27.050	0.365	0.415	1.136	0.963	I
C-R-245-4×4	245	28.898	33.390	0.248	0.564	2.270		I
C-R-250-4×4	250	33.208	39.957	0.046	0.732	15.973		IC
C-R-225-5×5	225	16.733	20.283	0.521	0.186	0.357		I
C-R-235-5×5	235	15.743	24.233	0.332	0.240	0.721		I
C-R-240-5×5	240	22.767	31.007	0.346	0.394	1.137	1.183	I
C-R-245-5×5	245	25.580	28.057	0.219	0.500	2.280		I
C-R-250-5×5	250	30.457	41.489	0.041	0.671	16.238		I
C-R-225-7×7	225	20.013	23.480	0.625	0.222	0.356		I
C-R-235-7×7	235	22.887	24.317	0.486	0.348	0.715		I
C-R-240-7×7	240	26.467	27.620	0.404	0.457	1.133	1.548	I
C-R-245-7×7	245	34.400	34.930	0.297	0.671	2.258		I
C-R-250-7×7	250	34.339	39.770	0.048	0.756	15.878		IC

[3] L_R – Length of the rock block; P_{ini} – Initial cracking load; P_{max} – Peak load; K_1^{ini} – Initial fracture toughness of mode 1; K_2^{ini} – Initial fracture toughness of mode 2; R_a – Degree of roughness; Failure mode "I" – Interfacial crack propagates through the interface; Failure mode "IC" – Sudden brittle failure near the supports at the same time when the interfacial crack propagates through the whole interface.

Table 4 Experimental results of the R-C series beams under FPS[4].

Specimen	L_R (mm)	P_{ini} (kN)	P_{max} (kN)	K_1^{ini} (MPa·m$^{1/2}$)	K_2^{ini} (MPa·m$^{1/2}$)	$\lvert K_2^{ini} / K_1^{ini} \rvert$	R_a (mm)	Failure mode
R-C-264-4×4	264	17.737	22.300	0.360	0.284	0.788	0.963	K
R-C-266-4×4	266	17.461	20.360	0.394	0.274	0.696		I
R-C-271-5×5	271	13.552	16.710	0.378	0.201	0.531	1.183	K
R-C-275-5×5	275	12.640	13.380	0.404	0.176	0.437		I

[4] L_R – Length of the rock block; P_{ini} – Initial cracking load; P_{max} – Peak load; K_1^{ini} – Initial fracture toughness of mode 1; K_2^{ini} – Initial fracture toughness of mode 2; R_a – Degree of roughness; Failure mode "I" – Propagation of the interfacial crack through the interface; Failure mode "K" – Initiation and propagation of the crack in the concrete.

Figures

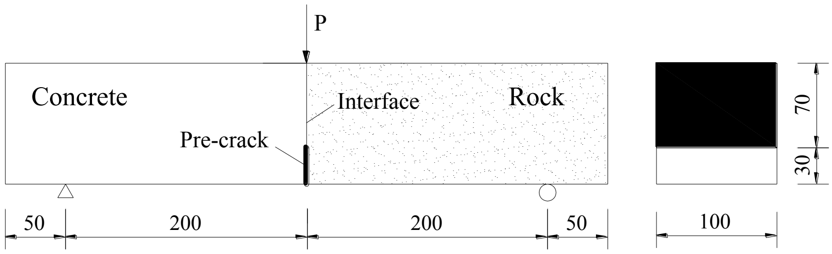

(a) Under three-point bending (TPB)

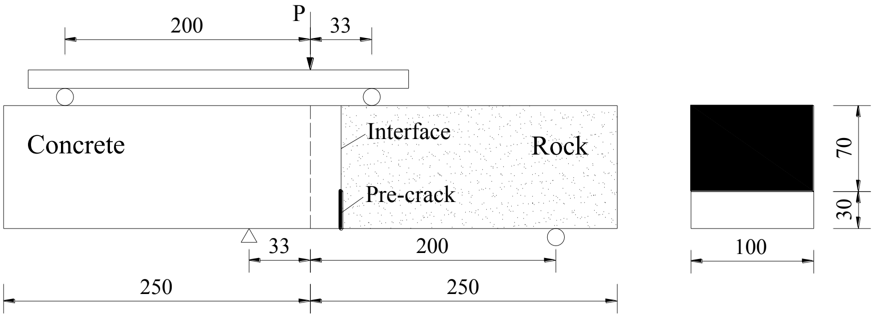

(b) Under four-point shear (FPS)

Fig. 1. Geometries of TPB and C-R series specimens for TPB and FPS fracture tests

(a) PVC film 1 pasted on the rock (b) PVC film 2 fixed using cello tape

Fig. 2. Preparation of the pre-crack

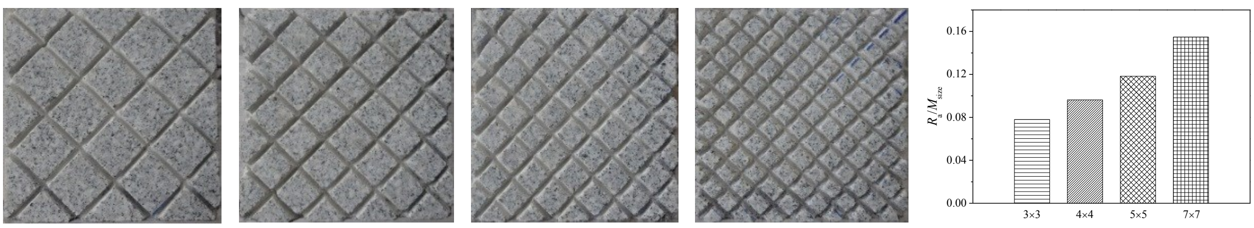

(a) 3×3 (b) 4×4 (c) 5×5 (d) 7×7 (e) R_a/M_{size}

Fig. 3. Features of rock surfaces at the interface

(a) TPB test (b) FPS test

Fig. 4. Experimental setups

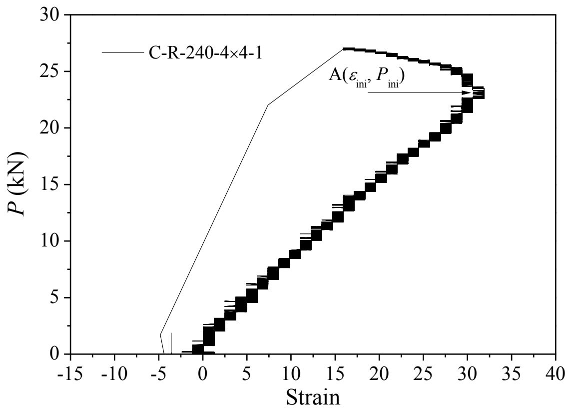

Fig. 5. Load versus strain curve for Specimen C-R-240-4×4-1

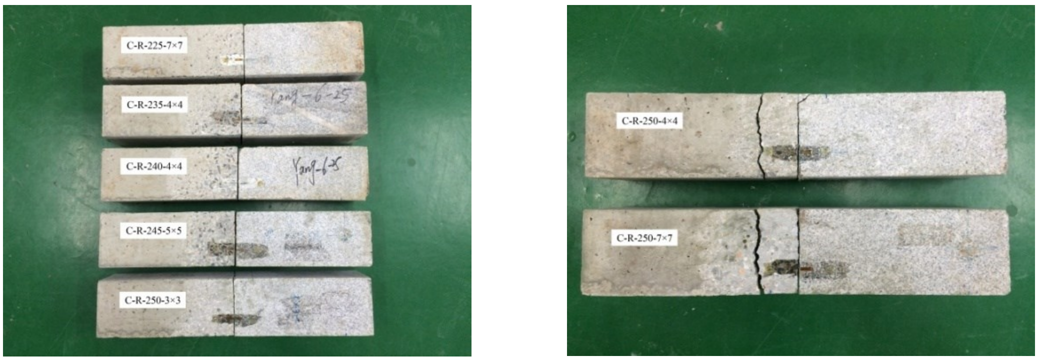

(a) Failure mode I (b) Failure mode IC

Fig. 6. Failure modes of C-R series specimens under FPS

Fig. 7. Cross-section of the specimen under interfacial failure

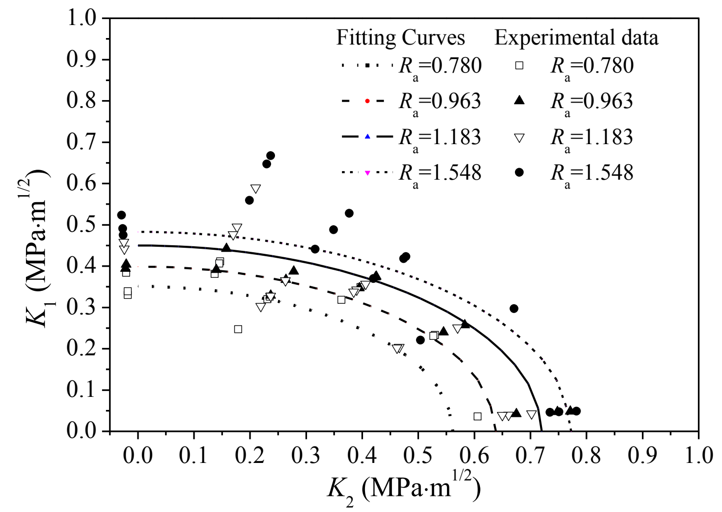

Fig. 8. K_1 versus K_2 relationships for interface crack initiation at four roughness degrees

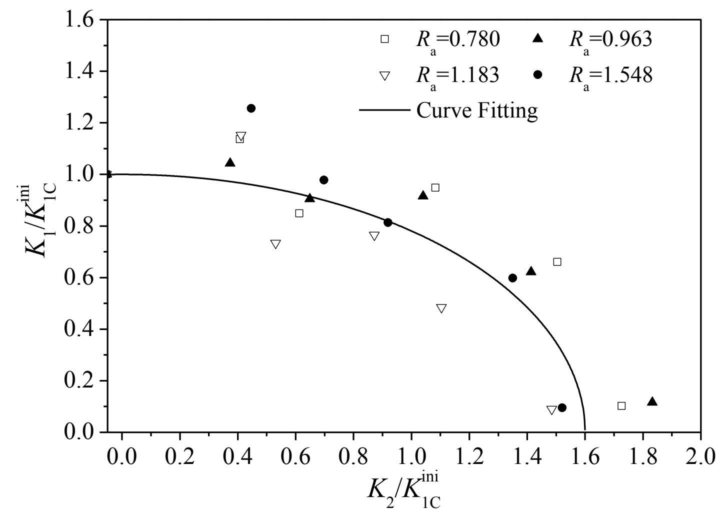

Fig. 9. Normalised K_1 versus K_2 relationships at interface crack initiation

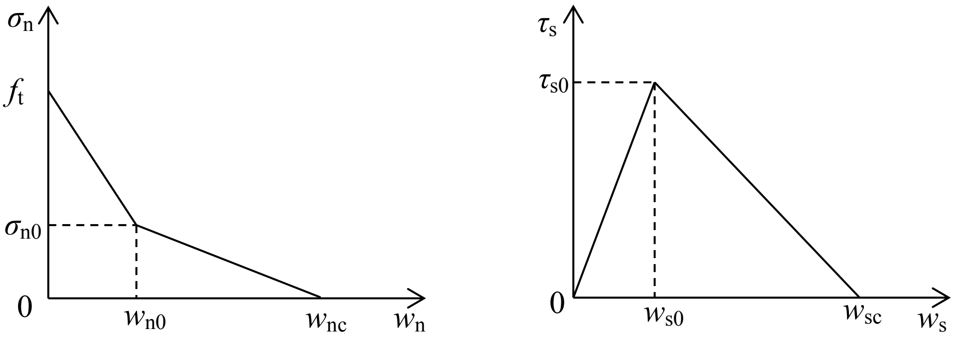

(a) Tension softening relationship (b) Shear softening relationship

Fig. 10. Cohesive tensile/shear stress versus displacement relationships

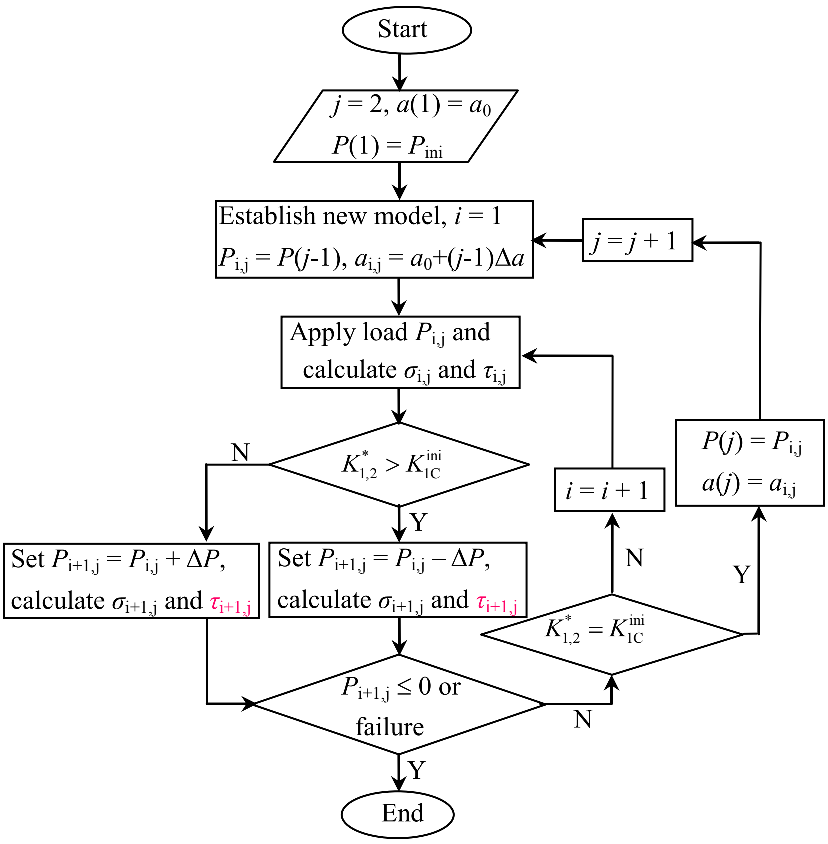

Fig. 11. Flow chart for numerical simulations

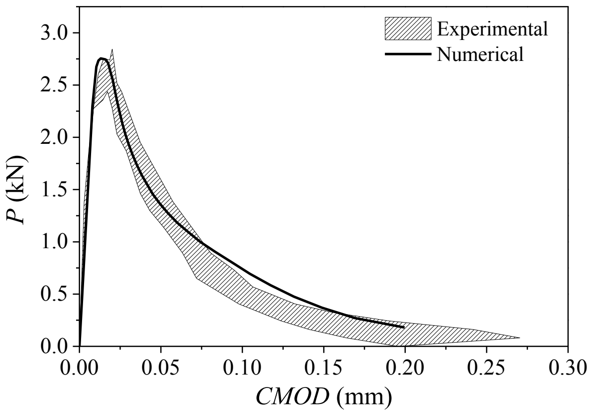

(a) Specimen TPB-5×5

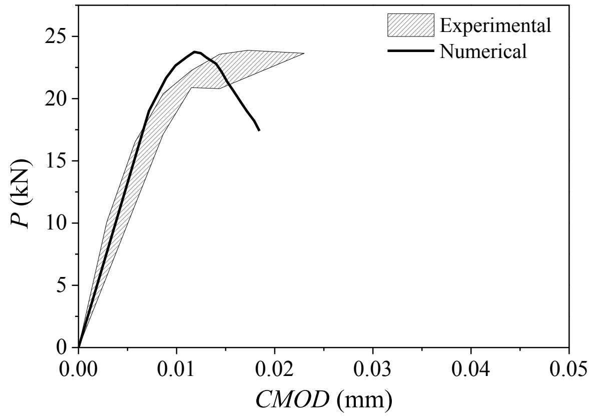

(b) Specimen C-R-240-3×3

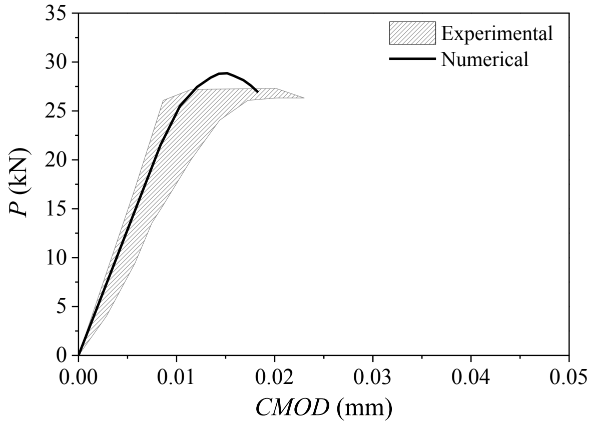

(c) Specimen C-R-240-4×4

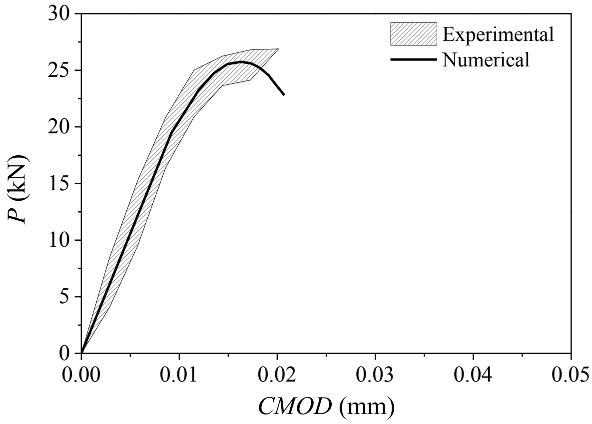

(d) Specimen C-R-235-5×5

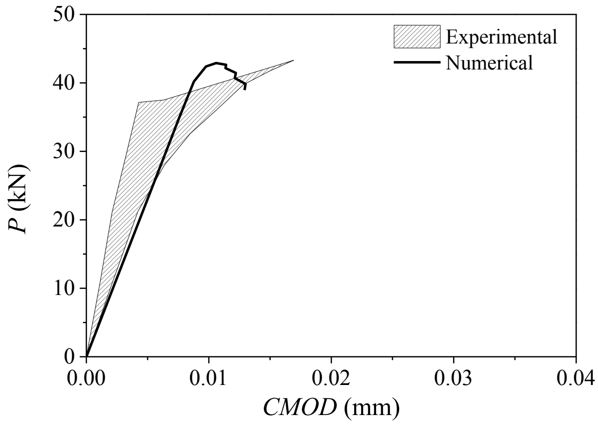

(e) Specimen C-R-250-7×7

Fig. 12. Comparisons of *P-CMOD* curves with the test data on TPB and C-R series specimens

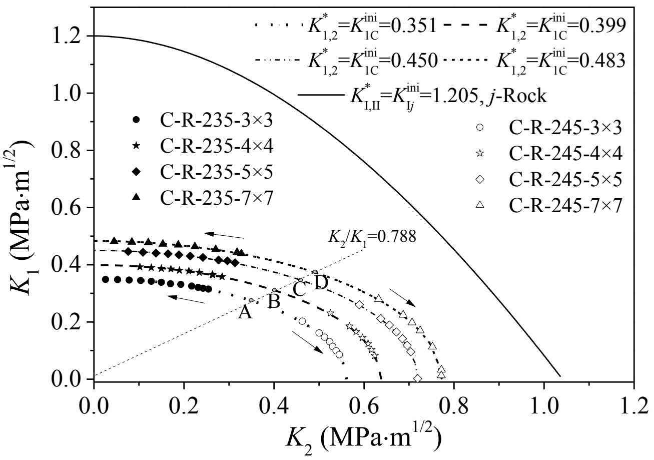

(a) Curves for the rock with $K^*_{\mathrm{I,II}} = K^{\mathrm{ini}}_{\mathrm{Ij}}$ and $K^*_{1,2} = K^{\mathrm{ini}}_{1\mathrm{C}}$

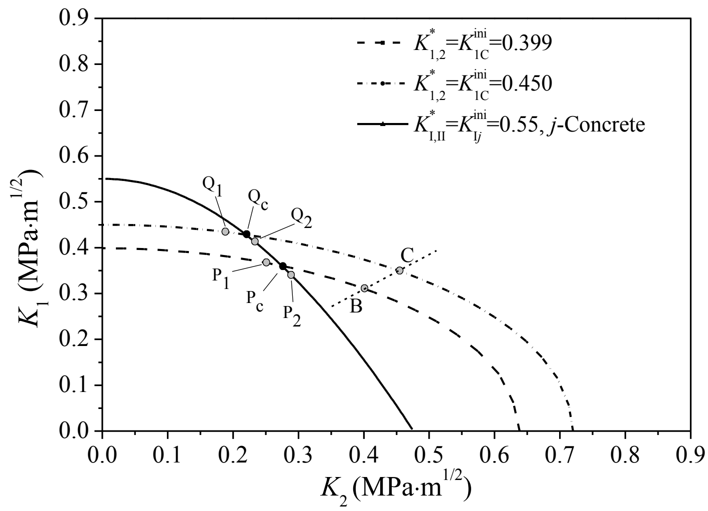

(b) Curves for the concrete with $K^*_{\mathrm{I,II}} = K^{\mathrm{ini}}_{\mathrm{Ij}}$ and $K^*_{1,2} = K^{\mathrm{ini}}_{1\mathrm{C}}$

Fig. 13. K_1 versus K_2 relationships for crack propagation criteria $K^*_{\mathrm{I,II}} = K^{\mathrm{ini}}_{\mathrm{Ij}}$ and $K^*_{1,2} = K^{\mathrm{ini}}_{1\mathrm{C}}$

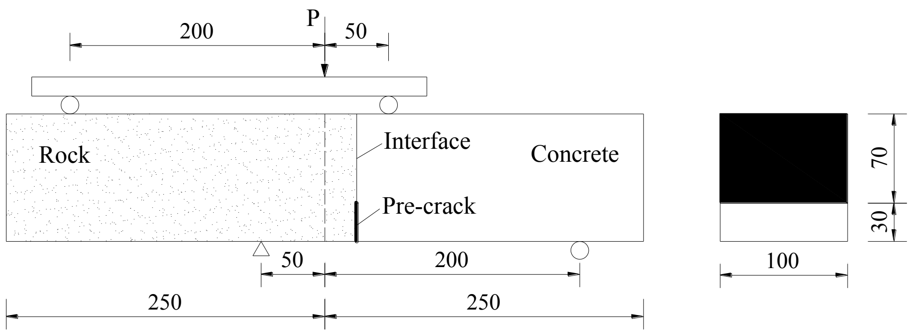

Fig. 14. Geometries of R-C series beams under four-point shear (FPS)

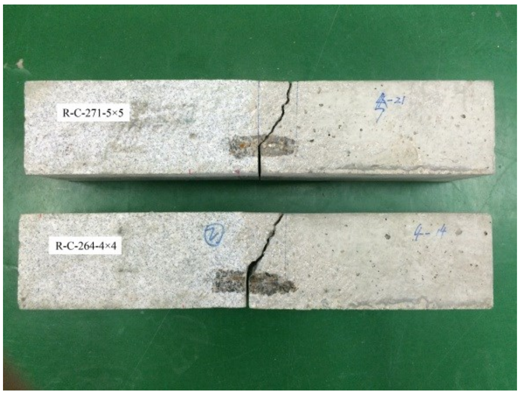

Fig. 15. Failure mode K of typical beams

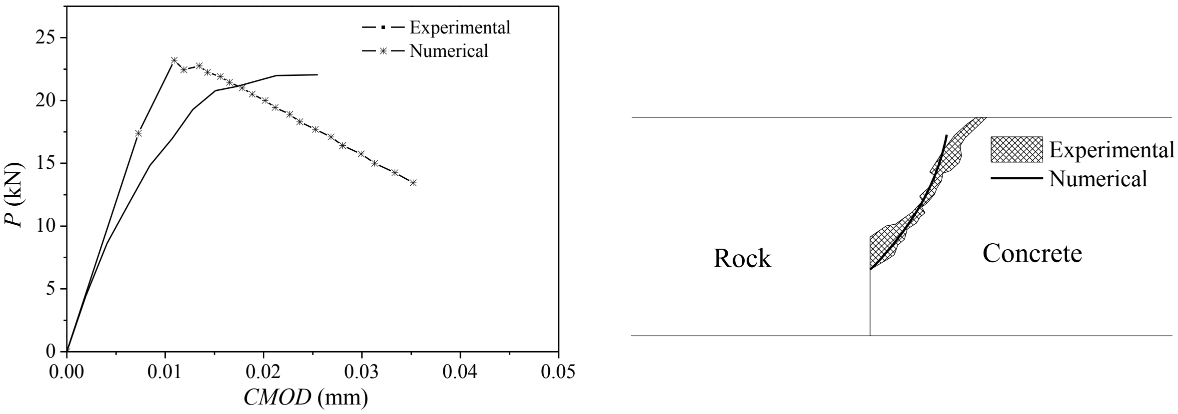

(a) *P-CMOD* curves

(b) Crack trajectories

Fig. 16. Comparisons of numerical *P-CMOD* curve and crack trajectory with the test data